Published in final edited form as:
Spine (Phila Pa 1976). 2011 April 1; 36(7): 512–520. doi:10.1097/BRS.0b013e3181f72b94.

Human Disc Nucleus Properties and Vertebral Endplate Permeability

Azucena G. Rodriguez, BS[1], **Chloe K. Slichter, BS**[1], **Frank L. Acosta, MD**[2], **Ana E. Rodriguez-Soto, BS**[3], **Andrew J. Burghardt, BS**[3], **Sharmila Majumdar, PhD**[3], and **Jeffrey C. Lotz, PhD**[1]

[1] Department of Orthopaedic Surgery, University of California, San Francisco, CA 94143, USA

[2] Department of Neurosurgery, Cedars-Sinai Medical Hospital, Los Angeles, CA 90048, USA

[3] Department of Radiology, University of California, San Francisco. San Francisco, CA 94143 USA

Abstract

Study of human cadaveric discs quantifying endplate permeability and porosity and correlating these with measures of disc quality: cell density, proteoglycan content, and overall degeneration. Permeability and porosity increased with age and were not correlated with cell density or overall degeneration, suggesting that endplate calcification may not accelerate disc degeneration.

Study Design—Experimental quantification of relationships between vertebral endplate morphology, permeability, disc cell density, glycosaminoglycan content and degeneration in samples harvested from human cadaveric spines.

Objective—To test the hypothesis that variation in endplate permeability and porosity contribute to changes in intervertebral disc cell density and overall degeneration.

Summary of Background Data—Cells within the intervertebral disc are dependent on diffusive exchange with capillaries in the adjacent vertebral bone. Previous findings suggest that blocked routes of transport negatively affect disc quality, yet there are no quantitative relationships between human vertebral endplate permeability, porosity, cell density and disc degeneration. Such relationships would be valuable for clarifying degeneration risk factors, and patient features that may impede efforts at disc tissue engineering.

Methods—Fifty-one motion segments were harvested from 13 frozen cadaveric human lumbar spines (32 to 85 years) and classified for degeneration using the MRI-based Pfirrmann scale. A cylindrical core was harvested from the center of each motion segment that included vertebral bony and cartilage endplates along with adjacent nucleus tissue. The endplate mobility, a type of permeability, was measured directly using a custom-made permeameter before and after the cartilage endplate was removed. Cell density within the nucleus tissue was estimated using the picogreen method while the nuclear GAG content was quantified using the DMMB technique. Specimens were imaged at 8 μm resolution using microCT, bony porosity was calculated. Analysis of variance, linear regression, and multiple comparison tests were used to analyze the data.

Results—Nucleus cell density increased as the disc height decreased (R^2=0.13; p=0.01) but was not related to subchondral bone porosity (p>0.5), total mobility (p>0.4) or age (p>0.2). When controlling for disc height however, a significant, negative effect of age on cell density was

Corresponding Author: Jeffrey C. Lotz, Ph.D., Department of Orthopaedic Surgery, University of California, San Francisco, 533 Parnassus Ave, U-453, Box 0514, San Francisco, CA 94143, fax: 415.476.1128, Ph: 415.476.7881, lotzj@orthosurg.ucsf.edu.

observed (p=0.03). In addition to this, GAG content decreased with age non-linearly (R^2=0.83, p<0.0001) and a cell function measurement, GAGs/cell decreased with degeneration (R^2=0.24; p<0.0001). Total mobility (R^2=0.14; p<0.01) and porosity (R^2=0.1, p<0.01) had a positive correlation with age.

Conclusion—Although cell density increased with degeneration, cell function indicated that GAGs/cell decreased. Since permeability and porosity increase with age and degeneration, this implies that cell dysfunction, rather than physical barriers to transport, accelerate disc disease.

Keywords

Disc degeneration; intervertebral disc; endplate permeability; porosity

Introduction

The intervertebral disc (IVD) loses its blood supply in the first decade of life.[1,2] This avascularity causes disc cells to rely on diffusion and convection for nutrient and metabolite exchange, principally with capillaries in the adjacent vertebral bodies.[3,4] Early work by Nachemson,[5] demonstrated that endplate capillaries are more numerous at the disc center, where the disc is tallest and cellular competition for nutrients is greatest.[6,7] The vertebral endplate has subsequently been shown to be the principal route for nucleus cell nutrition.[8,9]

Clearly, sustaining adequate transport is critical to disc health, as cells maintain the extracellular matrix (ECM) and regulate the biochemical environment.[10,11] Over thirty years ago, Nachemson hypothesized that endplate calcification may impede disc cell nutrition and lead to degeneration.5 Since then, this has been analyzed theoretically,12 and experimentally in vitro where a restriction in nutrient supply has been shown to reduce the number of viable or functional cells.[6] This notion is supported by several studies that report differences in diffusion pathways between healthy and degenerate discs.[13,14]

Transport linking endplate capillaries to disc cells is controlled by direction-dependent interactions between cartilage endplate and subchondral bone.[15,16] Hence, one mechanism for adversely affecting cell function is reduced cartilage permeability via calcification.[17,18] Alternatively, subchondral bone sclerosis may result in fewer and smaller pores through which transport can occur.[19] While qualitative evidence suggests one or more of these mechanisms underlie disc degeneration, quantifiable relationships between disc cellularity, endplate permeability, subchondral bone porosity, and matrix content are unavailable. Establishing such associations would help clarify disc degeneration pathomechanisms. Further, if degeneration is causally linked to transport inadequacy, then patient-specific risk factors that initially lead to degeneration may be detrimental for subsequent efforts at stimulating disc repair. That is, therapeutic increases in disc cell number and/or metabolic activity may not be achievable and sustainable within this transport constrained environment. The goal for this study was to investigate relationships between human endplate morphology, permeability, disc cell density, matrix content, and degeneration in attempts to establish quantitative relationships that would be useful for disc degeneration/regeneration research.

Materials and Methods

Dissection

Thirteen freshly frozen cadaveric human lumbar spines from levels L1–L5 and L1–L4 (age range 32–85 years; average age 63 ± 16 years; 4 females and 9 males) were obtained from donor banks. Overall, 51 motion segments were harvested. The specimens were kept at

−20°C until they were thawed for MRI assessment. The intervertebral disc (IVD) specimens were scanned in a 3T MRI Scanner (GE Healthcare, Milwaukee, WI) and graded by three trained radiologists using the Pfirrmann degeneration scale.[20] In order to obtain the average IVD height, three locations were selected and measured from mid-sagittal MRI images using NIH Image software: one from each lateral side and one at the center. The posterior processes were removed using a bone saw (Exakt Model 300, Band Saw, Norderstedt, Germany). Subsequently, the surrounding muscle and other soft tissue were dissected away from the spine. The motion segments were then cut transversely in each vertebra using a bone saw to obtain specimens consisting of half-vertebra/disc/half-vertebra (Figure 1). Next, they were refrozen for the following two steps, to preserve nuclear tissue. The motion segments were cored at the center of the nucleus pulposus using an 8.25 mm (inner diameter) diamond coring tool (Starlite Industries, Rosemont, PA) and a drill press. In the transverse plane, the center of the nucleus pulposus was approximated by marking a point one-third of the anterior-posterior length along the sagittal midline. Next, the adjacent vertebra/endplate core was separated from the nuclear tissue. In order to keep the cartilage endplate intact, the nucleus tissue was cut approximately 1 mm away from the cranial and caudal ends of the adjacent vertebra. Then, the nucleus was carefully divided in three roughly equal parts along the axial length of the nuclear core and labeled in reference to the adjacent vertebrae: superior, center and inferior (Figure 1). The 102 vertebral/endplate cores were stored at −20°C for later use in microCT imaging.

Imaging

The vertebral bone cores were thawed and imaged in a commercial micro-computed tomography system (μCT 40, Scanco Medical, Brüttisellen, Switzerland) with an X-ray tube voltage of 70 kV and 180o acquisition. Each core was placed in a cylindrical sample holder in a bath of protease inhibitors diluted 1:10 with distilled water (P2714 Protease inhibitor cocktail, Sigma-Aldrich, St Louis MO) to keep the cartilage in the specimens from degrading.21 A spatial resolution with an isotropic voxel size of 8 μm (matrix 2048 × 2048, 1000 projections/180o, FOV 16.4 mm) was chosen. Specimens were scanned along the length of each core, encompassing the vertebral endplate surface and 3 mm of bone underneath it. Next, image cross sections were reconstructed to create a 3D structure using the manufacturers' cone beam reconstruction algorithm.22 Then each 3D structure was transformed into 1000–1100 serial-8 μm thick-sliced images in a sagittal orientation. Next, a light Gaussian filter (to remove high frequency noise) followed by a fixed threshold was applied (to segment the images into a bone and pore phase).23 The irregular vertebral endplate surface was then identified using a custom made algorithm developed using MATLAB software. The semiautomatic technique is fully described elsewhere.24 For each sagittal μCT image, this algorithm identified a single region of interest (ROI) that included an 8 μm (one pixel) thick endplate surface contour. For each contour, the bone volume fraction (BV/TV) was calculated, where BV is bone volume and TV is tissue volume (equivalent to the ROI volume). The porosity was calculated as the average of 1-BV/TV for the series of sagittal images for each specimen.

Permeability testing

After the vertebral bone specimens were scanned, the specimens were trimmed to approximately 5 mm from the vertebral endplate surface using a low concentration diamond wafering blade on a Buehler Isomet Circular Low Speed Saw. The marrow was then removed from the trabecular bone using a water pik (Waterpik, CO) and the cores were stored at −20° C. A custom built permeameter was used to measure the permeability of the endplate cores. The permeameter consists of a series of pipes connected to a pressurized fluid reservoir (Figure 2) and was validated using porous stainless steel discs of known permeability (Mott Corp, Farmington, CT).[25]

Permeability measurements were performed on 51 vertebral/endplate cores, one from each motion segment. The locations inferior or superior were randomized and the matching core was saved for a future study. To assess the permeability of the cylindrical core samples, they were first thawed and then placed in perforated cryogenic vial caps (Cryogenic Vial, Corning Cat. No.2018). Then, cyanoacrylate glue was carefully added to seal the cartilage endplate periphery to prevent leaks around the specimen. The samples were oriented so that the driving hydraulic pressure was against the cartilage endplate so that fluid passed in the flow-out, disc to bone direction.[26] We chose the flow-out direction for two reasons. First, several groups have demonstrated that nucleus pressure compacts cartilage endplate leading to decreased matrix pore size and lower permeability.[26,27] Because of this, we adjusted the apparatus flow to correspond with physiologic disc pressures so cartilage endplate compaction in our experiment would match that present in vivo. In that way, we expect our data to be more representative of in situ conditions. A similar choice was made by other groups[28,29] and consequently this also allowed a representative comparison to historical data. Second, the cartilage endplate is only loosely adherent to the subchondral bone, and our preliminary attempts at measuring permeability in the flow-in direction damaged the specimens by separating tissues. The cartilaginous portion of the sample in the cryogenic vial was equilibrated in protease inhibitors diluted 1:10 in distilled water for half an hour to reduce cartilage degradation. The sample in the vial was then inserted in the sample mount and ready for testing. The permeameter was filled with deionized water and pressurized to 1 MPa – the average physiological pressure of the disc.[30] The fluid flow rate was calculated by measuring the weight of the fluid passing through the specimen at two-second intervals using a precision electronic balance (Ohaus, Cat No. AV2102CU-US, 2100g capacity, 0.01g resolution). The upstream fluid pressure (P_u) was generated using a nitrogen tank and was measured by a pressure sensor (Honeywell Sensotec, Columbus, Ohio, Model A-205). The downstream pressure (P_d) was atmospheric. Specimen's permeability (k) was calculated using Darcy's Law to relate the Darcy velocity (v) to the pressure drop across the specimen ($P_u - P_d$):

$$v = \frac{Q}{A} = \left(\frac{k}{\mu}\right)\left(\frac{P_u - P_d}{L_s}\right) \tag{1}$$

where Q is the flow rate (m^3/s), A is the cross-sectional area for fluid flow, μ is the fluid viscosity (Pa-s), the Darcy permeability constant k, is the intrinsic property of the tissue (m^2), and L_s is the specimen length (m). Each specimen's permeability was measured twice, once intact, and a second time; after careful removal of the cartilage endplate using blunt dissection and Toluidine blue tissue marker to differentiate the cartilage from the bone. The cartilaginous endplate thickness (L_{cep}) was then measured using a resistance micrometer.[31] The cartilage endplate permeability was calculated assuming 'permeabilities in series': that is, for the intact specimen, the flow is equal through both the cartilage endplate (cep) and subchondral bone (bone) (see also Figure 2):

$$Flow = \frac{Q_{cep}}{A} = \frac{Q_{bone}}{A} = \frac{Q_{total}}{A}$$
$$\frac{Q}{A} = \frac{Q_{cep}}{A} = \frac{k_{cep}}{\mu L_{cep}}(P_u - P_{d1}) = \frac{Q_{bone}}{A} = \frac{k_{bone}}{\mu L_{bone}}(P_{d1} - P_{d2}) = \frac{k_{total}}{\mu L_{total}}(P_u - P_{d2}) \tag{2}$$

From the intact specimen flow experiments, total permeability (k_{total}) in Equation 1 was determined. From the bone-only flow experiments, bone permeability (k_{bone}) was determined. Using these quantities, and the pressure-drop/flow-rate relationships from the intact specimen test, cartilage endplate permeability (k_{cep}) was determined from Equation 2 by first solving for P_{d1} and then for k_{cep}. The final results were reported in fluid mobility

units (m^4/N-s) and defined as the tissue permeability normalized by the viscosity of the fluid (k/μ).[32–34]

Biochemistry

Cell density was quantified by measuring DNA fluorescence using the Picogreen assay method (Molecular Probes Invitrogen Detection Technologies, Eugene, OR) following the manufacturer's protocol. First the stored nuclear tissue was thawed out for 3 minutes. Each nuclear section was finely minced, weighed to obtain wet weight, and then lyophilized in order to obtain dry weight. Samples were digested using papain (Sigma-Aldrich) prepared at a dilution of 1:100 in PBS for 24–36 hours at 60° C and then centrifuged at 3000 rpm for 10 minutes. After digestion, a pellet containing cells and supernatant containing GAGs were separated. The pellet was then resuspended in 300 mL of TE buffer (Sigma-Aldrich) and used to estimate nucleus cell density, while the supernatant was used to determine nucleus glycosaminoglycan (GAG) content. In a validation study, it was determined that the amount of DNA in the supernatant was negligible compared to the amount of DNA found in the pellet; for that reason the DNA was only obtained from the pellet. The amount of DNA was quantified by using the results from a standard curve produced using a calf thymus DNA concentration. Finally, the cell density was calculated by dividing the amount of DNA by 6 picograms of DNA which are contained per cell.[35]

Nucleus GAG content was quantified using the dimethylmethylene blue assay (DMMB) method with the supernatant from the nucleus digestion.[36] The supernant was diluted to 1:200 and then 40 μL of the solution was added to 250 μL of the DMMB dye solution. A wavelength reading was measured using a spectrophotometer (SpectraMax M3, Sunnyvale, CA). The GAG content was calculated based on a standard curve using an aqueous solution of chondroitin sulfate C from shark cartilage (chondroitin 6-sulfate, Sigma Aldrich, St. Louis, MO). The results were normalized by volume (mm^3) from the water content previously obtained.

Data Analysis

All statistical analyses were performed using the JMP (Version 7.0, SAS Institute Inc.). Interobserver variability was by determined by a kappa score. Means and standard deviations for the variables were obtained. Standard analysis of variance (ANOVA) and analysis of covariance (ANCOVA) procedures were performed to compare specimen group means and to estimate the effect of the specimen variables (degeneration grade entered as an ordinal predictor, and porosity, cartilage endplate thickness, and disc height entered as continuous predictors) on the measured parameters of interest (mobility, cell density, GAG content, GAGs/cell). When appropriate, Tukey post-hoc tests were used to identify group differences. Standard least squares multiple regression models were used to investigate relationships between variables, with the strength of association quantified by the correlation coefficient R^2.

Results

Of the 51 discs, 2 were scored Pfirrmann grade 1, 18 discs were grade 2, 21 were grade 3, 6 were grade 4, and 4 were grade 5. The disc tissue for one segment was subtracted because it was absent due to extreme degeneration. The calculated kappa value rating interobserver agreement on grading degenerative changes of the disc had a fair agreement with calculated k value of 0.41.

Endplate Mobility, Porosity & Cartilage Thickness

The mean total mobility was $3.26 \times 10^{-10} \pm 4.43 \times 10^{-10}$ m^4/N-s. For the cartilage endplate alone, the mobility was $1.19 \times 10^{-10} \pm 1.64 \times 10^{-10}$ m^4/N-s while that for the subchondral bone alone was $2.21 \times 10^{-9} \pm 1.37 \times 10^{-9}$ m^4/N-s. Total Mobility (TM) had a positive correlation with age and bone porosity (R^2=0.16, p<0.01; TM (x 10^{-10}) = 0.11*age − 3.80 and R^2=0.09, p=0.05; TM (x 10^{-10}) = 16.13*bone porosity − 5.33, respectively). Bone Mobility (BM) also had positive correlation with age and bone porosity (R^2=0.10, p=0.03; BM (x 10^{-10}) = 0.27*age + 4.89 and R^2=0.23, p<0.0001; BM (x 10^{-10}) = 75.15*bone porosity − 18.19, respectively). In addition, bone mobility had an inverse relationship with GAG content (R^2=0.16, p=0.004). The mean endplate porosity was 54.6 ± 7.5%, and was positively correlated with age (R^2=0.13, p<0.01, Figure 3) and degeneration (R^2=0.22, p=0.004). It was observed that cartilage thickness increased with age (R^2=0.08, p=0.03). A one-way repeated measures ANOVA indicated there was no statistically significant degeneration trend with spinal level with donor as a covariate (p=0.94).

Cell density

The mean cell density was 1651 ± 1015 cells/mm^3 (Table 1). The results of the one way repeated measures ANOVA demonstrated that the three cell density regions were not statistically different. Therefore the average cell density was used. There was a significant decrement between grade 1 and 2 discs, then a progressive increase with degeneration grades 2 through 5 (Figure 4). When specimen factors were analyzed individually, cell density decreased as disc height increased (R^2=0.13 p<0.02), but was not directly related to subchondral bone porosity (p>0.5), total mobility (p>0.4), or age (p>0.2). Assuming an exponential relationship between cell density and disc height[7] gives

$$CD = 16324 \times h^{-1.02}$$

where, CD is cell density (cells per mm^3), and h is disc height (mm); (R^2=0.15, p=0.005, Figure 5). When controlling for disc height, cell density was inversely correlated to age (R^2=0.26, p<0.003).

GAGs

The results of the one way repeated measures ANOVA demonstrated that the three GAG content regions were not statistically different. Therefore, the average cell density was used. Average GAG content non-linearly decreased with age (R^2=0.83, p<0.0001; average GAG=230118*$age^{-2.49}$, Figure 6) and Pfirrmann grade (R^2=0.52, p<0.0001), with grade 1 significantly higher than grades 2–5, and grade 4 being significantly lower than grades 1 and 2. When controlling for age, GAG content did not depend on endplate permeability (p>0.05). However, endplate porosity decreased as GAG content increased (R^2=0.20, p<0.002). Disc height was non-linearly correlated with average GAG content, where height decreased precipitously when GAG content was below 10 μg/mm^3 (R^2=0.20; p<0.001).

GAGs/cell

GAG content was normalized by cell density as an indirect measure of cell function. Average GAGs/cell decreased with degeneration, with statistically-significant differences between grades 1–3 and grade 4–5 (R^2=0.24; p<0.0001, Figure 7). It was also weakly correlated with disc height (R^2=0.17, p<0.01) and inversely correlated with age (R^2=0.14, p<0.01). There was no relationship with mobility (p>0.3), or porosity (p>0.07). When modeled together, disc height and age explained 25% of the variation of GAGs/cell

(p=0.001). When GAGs/cell was calculated for the endplate-adjacent regions only, this was weakly inversely correlated with adjacent bone porosity (R^2=0.05, p=0.04).

Degeneration

Pfirrmann grade increased with age (R^2=0.31, p=0.002), with grades 1, 3 & 4 being statistically different. With increasing degeneration, subchondral bone porosity increased (R^2=0.22; p<0.0004) and disc height decreased: height of grade 3 discs was less than grade 2, and grade 4 and 5 discs were less than grades 2 and 3 (R^2=0.57, p<0.0001).

Discussion

Our goal was to investigate how disc endplate features correlate with disc cellularity and degeneration within the context of our broader objective to learn whether transport limitations can impede disc tissue engineering. We observed that disc cellularity was inversely correlated with disc height, increased with progressive degeneration beyond grade 2, and was unrelated to cartilage endplate mobility or subchondral bone porosity. Although cell density increased with degeneration, cell function indicated by GAGs/cell decreased. Importantly, we noted that total endplate mobility and porosity increase with age and degeneration. Taken together, these results imply that cell dysfunction, rather than physical barriers to transport, accelerates disc disease.

There was also an interesting interplay between age, endplate bone porosity, and GAG content. We observed that endplate porosity increased with age while GAG content decreased. These opposing trends in porosity and GAG content conflict with reports by Nachemson who made qualitative observations on a smaller sample of endplates and noted a porosity decreased with age and degeneration.[5] More recently, Benneker and coworkers quantified endplate pores in 2 mm thick endplate samples and also reported a decrease in the density of holes (20 to 50 μm range) with increasing degeneration and GAG content, and a variable relationship with age.[37] The discrepancy with our results may be due to their focus on a narrow range of hole sizes, as they note that overall hole density did not correlate with degeneration because of the presence of large openings that were more apparent with grade 4 and 5 discs. Other authors have reported that increasing GAG content is associated with increased endplate thickness, stiffness, and presumably decreased porosity, and that this may be due to vertebral remodeling to balance increased nuclear osmotic swelling.[38–40] While it is well recognized that GAG content decreases with degeneration,[41] these results collectively support our finding that endplate porosity increases with age, and that this may be an adaptive response to a reduction of nuclear swelling pressure.

Mobility has been reported for endplates from several species. Baboon cartilage endplate mobility was measured using confined compression and reported to be 14.3×10^{-14} m^4/Ns cartilage.[21] Accadbled and colleagues measured mobility of intact endplates from growing lambs and pigs that ranged from 1.32×10^{-14} m^4/N-s (lamb) to 3.69×10^{-14} m^4/Ns (pig).[28,42] Our total mobility (3.26×10^{-10} m^4/N-s) and cartilage mobility (1.19×10^{-10} m^4/N-s) values were significantly higher, likely due to inhomogeneities and focal cartilage lesions common in degenerated human samples. Conversely, our endplate bone mobility values ($2.21 \pm 1.37 \times 10^{-9}$ m^4/N-s) are lower than those reported by others for human bone removed from the vertebral centrum (3.52×10^{-6} m^4/N-s).[43] This difference is likely due to the fact that our samples included the bony endplate.

Cell density was inversely-related to disc height. This observation is consistent with the well-established concept that diffusive transport (and consequently diffusion distance) is a crucial factor for disc cell viability.[6,44] Stairmand et al. presented an inverse power relationship ($h^{-0.675}$) between cell density and half-disc height across several species and a

large range of disc sizes.[7] Over our narrower range (5.8–15.7 mm), cell density was nearly proportional to height, yet the weak association (R^2=0.15) suggests other factors play an important role, such as age, that explains another 10% of the variance. Yet, historical reports linking cell density to age have been mixed. Maroudas et al. showed that cell density increased with age in the three samples investigated, while Liebscher et al. did not find a strong correlation between cell density and age for donors older than 16 years of age.[45,46] Our results demonstrate that the strong influence of disc height needs to be considered in statistical analyses; otherwise the strength of other associations may be missed. Discrepancies with historical data may also be differences in cell density analysis techniques: our average nucleus cell density was approximately 1700 cells/mm^3, while others report this to be closer to 4000 cells/mm^3.[46,47] We estimated cell density by quantification of DNA, while others typically rely on histological methods and extrapolation from two-dimensional images to volumetric estimates.

Our report of increasing endplate porosity with degeneration is at odds with a common clinical view that degenerate discs have more sclerotic endplates. For example, subchondral bone sclerosis (and presumably decreased endplate porosity) has been identified as a characteristic of spine osteoarthritis,[48] and given the tenuous nature of disc cell nutrition, this sclerosis would negatively impact disc health.49 Yet, while radiographic evidence of moderate sclerosis is evident in some low back pain patients, no dose-response relationship is apparent.50 Conversely, some have argued that moderate osteoporosis would be protective against disc degeneration.51 However, the clinical data relating osteoporosis to degeneration are mixed,52 with no clear evidence that osteoporosis either protects against or predisposes to degeneration. In a more direct assessment of endplate structure and disc degeneration, Grant and colleagues measured the strength of 77 human endplates using an indentation protocol. They report that endplate strength was correlated with vertebral BMD, and that increasing disc degeneration was associated with an overall loss of endplate strength. Consistent findings were reported by Keller and coworkers,[38] who observed a significant negative correlation between endplate stiffness and increasing disc degeneration. Consequently, while vertebral rim density is consistently increased with disc degeneration (i.e. osteophytes), our observations are supported by biomechanical data and indicate that the central endplate becomes more porous with disc degeneration.

Our study is limited because measurements were made on cadaveric tissues and cause-and-effect cannot be directly established. As such, we can only report trends or associations between variables and hypotheses regarding mechanisms are not testable. Equally important, vertebral capillary density was not calculated and therefore the role of nutrition on disc cell density or degeneration cannot be fully clarified. It is well established that many factors, such as smoking, diabetes, atherosclerosis, or steroid use, can decrease vertebral blood flow that, in turn, can impair cell function and accelerate disc degeneration.[53–56] Because these co-morbidities are common in the general population, it is likely that vertebral capillary density varies significantly between individuals and needs to be analyzed in future studies. In this regard, studies using imageable tracers may be particularly valuable.[57]

Another protocol limitation was measurement of mobility in the flow-out direction only. Because the cartilage endplate is supported by subchondral bone on one side, the resistance to fluid flow is direction dependent.[16,26] Here, the flow-out direction was chosen so that test fluid pressure would compact the cartilage endplate analogous to the in vivo situation. Ultimately, disc nutrition is mainly facilitated by movement of small molecules (e.g. glucose) along a concentration gradient (diffusion) rather than fluid flow along a pressure gradient (convection).[49,58] Nonetheless, the mobility that characterizes the resistance to solvent flow during convection and the filtration coefficient that quantifies resistance to solute flow during diffusion co-vary since they are both related to tissue pore size.59

Accordingly, in these experiments it was more important to compact the cartilage endplate so that the tissue pore size corresponded to in vivo conditions rather than quantify direction-dependent mobility.

Successful intervertebral disc tissue engineering requires a stable physicochemical environment.60 Given this diffusion-limited system, nucleus oxygen is very sensitive to cell density and cell metabolism.7 Diminished oxygen, in turn, is known to adversely influence disc cell function.[61] Our data suggest that changes in endplate mobility or porosity are not sealing off the disc from vertebral capillaries since mobility and porosity increase with age and degeneration, and our mean porosity (54.6%) is far from the theoretical value of 20% suggested by others to provoke disc cell dysfunction.[62] Alternatively, age-related decreases in GAG content and GAGs/cell indicate cellular dysfunction that may be due to senescence, 63 or as mentioned above, a poor capillary nutritional source rather than endplate pathology. The majority of current tissue engineering strategies focus on stimulating disc cell matrix synthesis using growth factors,64 or augmenting the nucleus with rejuvenated cells.[65,66] Conceptually, these therapies will stress homeostasis and place increased demands on available nutrition routes. For these approaches to be successful therefore, the system needs to have excess capacity to achieve a new steady-state that will sustain increased cell metabolism. This may be the case as transplantation of disc cells and growth factors has begun and shows some clinical benefit in canine models.[67,68]

In summary, our results solidify well-established concepts that disc degeneration is associated with age-related decreases in GAG content and cell activity. The strong influence of disc height on cell density suggests a compensatory mechanism that may help maintain disc cellularity as degeneration progresses. Unexpectedly, endplate mobility and porosity were found to increase with age and degeneration. These observations are important both for better understanding degeneration mechanisms but also for evaluating potential risks for regenerative therapies. The preservation of mobility and porosity indicates the disc may not be a ‘coffin’,[69] and implicates other factors as more important for contributing to the degeneration cascade, such as cell senescence or loss of vertebral blood supply.

Key points

- Endplate permeability and porosity increased with age and degeneration
- Disc cell density correlated inversely with disc height and increased in later stages of disc degeneration
- Proteoglycan content decreased non-linearly with age and degeneration
- GAG content per cell decreased with age and degeneration
- These data suggest endplate hypermineralization does not accelerate disc degeneration

Acknowledgments

Acknowledge NIH Grant: RO1AR052811

The authors thank David Schultz for assistance with the design of the permeameter and David Lari for assistance with the illustrations.

References

1. Boos N, Weissbach S, Rohrbach H, et al. Classification of age-related changes in lumbar intervertebral discs: 2002 Volvo Award in basic science. Spine. 2002; 27:2631–44. [PubMed: 12461389]
2. Crock, HV.; Goldwasser, M.; Yoshizawa, H. Vascular anatomy related to the intervertebral disc. In: Ghosh, P., editor. The Biology of the intervertebral disc. Boca Raton, FL: CRC Press; 1988. p. 109-33.
3. Boos N, Wallin A, Schmucker T, et al. Quantitative MR imaging of lumbar intervertebral disc and vertebral bodies: methodology, reproducibility, and preliminary results. Magn Reson Imaging. 1994; 12:577–87. [PubMed: 8057762]
4. Urban JP, Holm S, Maroudas A. Diffusion of small solutes into the intervertebral disc: as in vivo study. Biorheology. 1978; 15:203–21. [PubMed: 737323]
5. Nachemson A, Lewin T, Maroudas A, et al. In vitro diffusion of dye through the end-plates and the annulus fibrosus of human lumbar inter-vertebral discs. Acta Orthop Scand. 1970; 41:589–607. [PubMed: 5516549]
6. Horner HA, Urban JP. 2001 Volvo Award Winner in Basic Science Studies: Effect of nutrient supply on the viability of cells from the nucleus pulposus of the intervertebral disc. Spine. 2001; 26:2543–9. [PubMed: 11725234]
7. Stairmand JW, Holm S, Urban JP. Factors influencing oxygen concentration gradients in the intervertebral disc. A theoretical analysis. Spine. 1991; 16:444–9. [PubMed: 2047917]
8. Holm S, Maroudas A, Urban JP, et al. Nutrition of the intervertebral disc: solute transport and metabolism. Connect Tissue Res. 1981; 8:101–19. [PubMed: 6453689]
9. Ogata K, Whiteside LA. 1980 Volvo award winner in basic science. Nutritional pathways of the intervertebral disc. An experimental study using hydrogen washout technique. Spine. 1981; 6:211–6. [PubMed: 7268543]
10. Bibby SR, Jones DA, Ripley RM, et al. Metabolism of the intervertebral disc: effects of low levels of oxygen, glucose, and pH on rates of energy metabolism of bovine nucleus pulposus cells. Spine. 2005; 30:487–96. [PubMed: 15738779]
11. Bibby SR, Meir A, Fairbank JC, et al. Cell viability and the physical environment in the scoliotic intervertebral disc. Stud Health Technol Inform. 2002; 91:419–21. [PubMed: 15457768]
12. Soukane DM, Shirazi-Adl A, Urban JP. Computation of coupled diffusion of oxygen, glucose and lactic acid in an intervertebral disc. J Biomech. 2007; 40:2645–54. [PubMed: 17336990]
13. Antoniou J, Goudsouzian NM, Heathfield TF, et al. The human lumbar endplate. Evidence of changes in biosynthesis and denaturation of the extracellular matrix with growth, maturation, aging, and degeneration. Spine. 1996; 21:1153–61. [PubMed: 8727189]
14. Gu WY, Mao XG, Foster RJ, et al. The anisotropic hydraulic permeability of human lumbar anulus fibrosus. Influence of age, degeneration, direction, and water content. Spine. 1999; 24:2449–55. [PubMed: 10626306]
15. Ayotte DC, Ito K, Perren SM, et al. Direction-dependent constriction flow in a poroelastic solid: the intervertebral disc valve. J Biomech Eng. 2000; 122:587–93. [PubMed: 11192378]
16. Riches PE, Dhillon N, Lotz J, et al. The internal mechanics of the intervertebral disc under cyclic loading. J Biomech. 2002; 35:1263–71. [PubMed: 12163315]
17. Bernick S, Cailliet R. Vertebral end-plate changes with aging of human vertebrae. Spine. 1982; 7:97–102. [PubMed: 7089697]
18. Roberts S, Menage J, Eisenstein SM. The cartilage end-plate and intervertebral disc in scoliosis: calcification and other sequelae. J Orthop Res. 1993; 11:747–57. [PubMed: 8410475]
19. Benneker LM, Heini PF, Anderson SE, et al. Correlation of radiographic and MRI parameters to morphological and biochemical assessment of intervertebral disc degeneration. Eur Spine J. 2005; 14:27–35. [PubMed: 15723249]
20. Pfirrmann CW, Metzdorf A, Zanetti M, et al. Magnetic resonance classification of lumbar intervertebral disc degeneration. Spine. 2001; 26:1873–8. [PubMed: 11568697]
21. Setton LA, Zhu W, Weidenbaum M, et al. Compressive properties of the cartilaginous end-plate of the baboon lumbar spine. J Orthop Res. 1993; 11:228–39. [PubMed: 8483035]

22. Nazarian A, Snyder BD, Zurakowski D, et al. Quantitative micro-computed tomography: a non-invasive method to assess equivalent bone mineral density. Bone. 2008; 43:302–11. [PubMed: 18539557]
23. Burghardt AJ, Kazakia GJ, Majumdar S. A local adaptive threshold strategy for high resolution peripheral quantitative computed tomography of trabecular bone. Ann Biomed Eng. 2007; 35:1678–86. [PubMed: 17602299]
24. Rodríguez-Soto, AE.; Rodríguez, AG.; Burghardt, A., et al. Automatic Segmentation of the Vertebral Endplate VOI from Micro-CT Images. 2010. Manuscript in progress
25. Rodriguez, AG.; Schultz, DS.; Lotz, JC. Permeameter Device Validation. 2010. Manuscript in progress
26. Ayotte DC, Ito K, Tepic S. Direction-dependent resistance to flow in the endplate of the intervertebral disc: an ex vivo study. J Orthop Res. 2001; 19:1073–7. [PubMed: 11781007]
27. Dhillon N, Bass EC, Lotz JC. Effect of frozen storage on the creep behavior of human intervertebral discs. Spine. 2001; 26:883–8. [PubMed: 11317110]
28. Accadbled F, Laffosse JM, Ambard D, et al. Influence of location, fluid flow direction, and tissue maturity on the macroscopic permeability of vertebral end plates. Spine. 2008; 33:612–9. [PubMed: 18344854]
29. Setton LA, Chen J. Cell mechanics and mechanobiology in the intervertebral disc. Spine. 2004; 29:2710–23. [PubMed: 15564920]
30. Nachemson A. The load on lumbar disks in different positions of the body. Clin Orthop Relat Res. 1966; 45:107–22. [PubMed: 5937361]
31. Wagner DR, Lotz JC. Theoretical model and experimental results for the nonlinear elastic behavior of human annulus fibrosus. J Orthop Res. 2004; 22:901–9. [PubMed: 15183453]
32. Al-Munajjed AA, Hien M, Kujat R, et al. Influence of pore size on tensile strength, permeability and porosity of hyaluronan-collagen scaffolds. J Mater Sci Mater Med. 2008; 19:2859–64. [PubMed: 18347950]
33. Ayan C, Colley N, Cowan G, et al. Measuring Permeability Anisotropy - the Latest Approach. Oilfield Review. 1994; 6:24–35.
34. O'Brien FJ, Harley BA, Waller MA, et al. The effect of pore size on permeability and cell attachment in collagen scaffolds for tissue engineering. Technol Health Care. 2007; 15:3–17. [PubMed: 17264409]
35. Kim YJ SR, Doong JY, Grodzinsky AJ. Fluorometric assay of DNA in cartilage explants using Hoechst 33258. Anal Biochem. 1988; 174:168–76. [PubMed: 2464289]
36. Farndale RW, Buttle DJ, Barrett AJ. Improved quantitation and discrimination of sulphated glycosaminoglycans by use of dimethylmethylene blue. Biochim Biophys Acta. 1986; 883:173–7. [PubMed: 3091074]
37. Benneker LM, Heini PF, Alini M, et al. 2004 Young Investigator Award Winner: vertebral endplate marrow contact channel occlusions and intervertebral disc degeneration. Spine. 2005; 30:167–73. [PubMed: 15644751]
38. Keller TS, Ziv I, Moeljanto E, et al. Interdependence of lumbar disc and subdiscal bone properties: a report of the normal and degenerated spine. J Spinal Disord. 1993; 6:106–13. [PubMed: 8504221]
39. Resnick, D.; Niwayama, G. Degenerative disease of the spineed. Saunders; Philadelphia: 1981.
40. Roberts N, Gratin C, Whitehouse GH. MRI analysis of lumbar intervertebral disc height in young and older populations. J Magn Reson Imaging. 1997; 7:880–6. [PubMed: 9307915]
41. Urban JP, McMullin JF. Swelling pressure of the lumbar intervertebral discs: influence of age, spinal level, composition, and degeneration. Spine. 1988; 13:179–87. [PubMed: 3406838]
42. Accadbled F, Ambard D, de Gauzy JS, et al. A measurement technique to evaluate the macroscopic permeability of the vertebral end-plate. Med Eng Phys. 2008; 30:116–22. [PubMed: 17446114]
43. Nauman EA, Fong KE, Keaveny TM. Dependence of intertrabecular permeability on flow direction and anatomic site. Ann Biomed Eng. 1999; 27:517–24. [PubMed: 10468236]

44. Urban JP. The role of the physicochemical environment in determining disc cell behaviour. Biochem Soc Trans. 2002; 30:858–64. [PubMed: 12440933]
45. Liebscher, T.; Wuertz, K.; Haefeli, M., et al. Orthopaedic Research Society. Las Vegas, NV. U.S.A: 2009. Age-Associated changes in the cell number of the human lumbar intervertebral disc.
46. Maroudas A. Biophysical chemistry of cartilaginous tissues with special reference to solute and fluid transport. Biorheology. 1975; 12:233–48. [PubMed: 1106795]
47. Hastreiter D, Ozuna RM, Spector M. Regional variations in certain cellular characteristics in human lumbar intervertebral discs, including the presence of alpha-smooth muscle actin. J Orthop Res. 2001; 19:597–604. [PubMed: 11518268]
48. Jacobson JA, Girish G, Jiang Y, et al. Radiographic evaluation of arthritis: degenerative joint disease and variations. Radiology. 2008; 248:737–47. [PubMed: 18710973]
49. Urban JP, Smith S, Fairbank JC. Nutrition of the intervertebral disc. Spine. 2004; 29:2700–9. [PubMed: 15564919]
50. Pye SR, Reid DM, Adams JE, et al. Radiographic features of lumbar disc degeneration and bone mineral density in men and women. Ann Rheum Dis. 2006; 65:234–8. [PubMed: 16014671]
51. Margulies JY, Payzer A, Nyska M, et al. The relationship between degenerative changes and osteoporosis in the lumbar spine. Clin Orthop Relat Res. 1996:145–52. [PubMed: 8595750]
52. Aoki J, Yamamoto I, Kitamura N, et al. End plate of the discovertebral joint: degenerative change in the elderly adult. Radiology. 1987; 164:411–4. [PubMed: 3602378]
53. Holm S, Nachemson A. Nutrition of the intervertebral disc: acute effects of cigarette smoking. An experimental animal study. Ups J Med Sci. 1988; 93:91–9. [PubMed: 3376356]
54. Iwashina T, Mochida J, Sakai D, et al. Feasibility of using a human nucleus pulposus cell line as a cell source in cell transplantation therapy for intervertebral disc degeneration. Spine. 2006; 31:1177–86. [PubMed: 16688029]
55. Jhawar BS, Fuchs CS, Colditz GA, et al. Cardiovascular risk factors for physician-diagnosed lumbar disc herniation. Spine J. 2006; 6:684–91. [PubMed: 17088199]
56. Oda H, Matsuzaki H, Tokuhashi Y, et al. Degeneration of intervertebral discs due to smoking: experimental assessment in a rat-smoking model. J Orthop Sci. 2004; 9:135–41. [PubMed: 15045541]
57. Rajasekaran S, Babu JN, Arun R, et al. ISSLS prize winner: A study of diffusion in human lumbar discs: a serial magnetic resonance imaging study documenting the influence of the endplate on diffusion in normal and degenerate discs. Spine. 2004; 29:2654–67. [PubMed: 15564914]
58. Katz MM, Hargens AR, Garfin SR. Intervertebral disc nutrition. Diffusion versus convection. Clin Orthop Relat Res. 1986:243–5. [PubMed: 3757370]
59. Villars, FMH.; Benedek, GB. Physics wiht illustrative examples from medicine and biology. Reading, Mass: Addison-Wesley; 1974. Diffusion and transport processes.
60. Takeno K, Kobayashi S, Negoro K, et al. Physical limitations to tissue engineering of intervertebral disc cells: effect of extracellular osmotic change on glycosaminoglycan production and cell metabolism. Laboratory investigation. J Neurosurg Spine. 2007; 7:637–44. [PubMed: 18074689]
61. Ishihara H, Urban JP. Effects of low oxygen concentrations and metabolic inhibitors on proteoglycan and protein synthesis rates in the intervertebral disc. J Orthop Res. 1999; 17:829–35. [PubMed: 10632449]
62. Guehring T, Wilde G, Sumner M, et al. Notochordal intervertebral disc cells: sensitivity to nutrient deprivation. Arthritis Rheum. 2009; 60:1026–34. [PubMed: 19333932]
63. Roberts S, Evans H, Trivedi J, et al. Histology and pathology of the human intervertebral disc. J Bone Joint Surg Am. 2006; 88 (Suppl 2):10–4. [PubMed: 16595436]
64. Masuda K. Biological repair of the degenerated intervertebral disc by the injection of growth factors. Eur Spine J. 2008; 17 (Suppl 4):441–51. [PubMed: 19005698]
65. Kandel R, Roberts S, Urban JP. Tissue engineering and the intervertebral disc: the challenges. Eur Spine J. 2008; 17 (Suppl 4):480–91. [PubMed: 19005701]
66. Sobajima S, Vadala G, Shimer A, et al. Feasibility of a stem cell therapy for intervertebral disc degeneration. Spine J. 2008; 8:888–96. [PubMed: 18082460]

67. Hohaus C, Ganey TM, Minkus Y, et al. Cell transplantation in lumbar spine disc degeneration disease. Eur Spine J. 2008; 17 (Suppl 4):492–503. [PubMed: 19005697]

68. Meisel HJ, Siodla V, Ganey T, et al. Clinical experience in cell-based therapeutics: disc chondrocyte transplantation A treatment for degenerated or damaged intervertebral disc. Biomol Eng. 2007; 24:5–21. [PubMed: 16963315]

69. Johnson WE, Roberts S. 'Rumours of my death may have been greatly exaggerated': a brief review of cell death in human intervertebral disc disease and implications for cell transplantation therapy. Biochem Soc Trans. 2007; 35:680–2. [PubMed: 17635120]

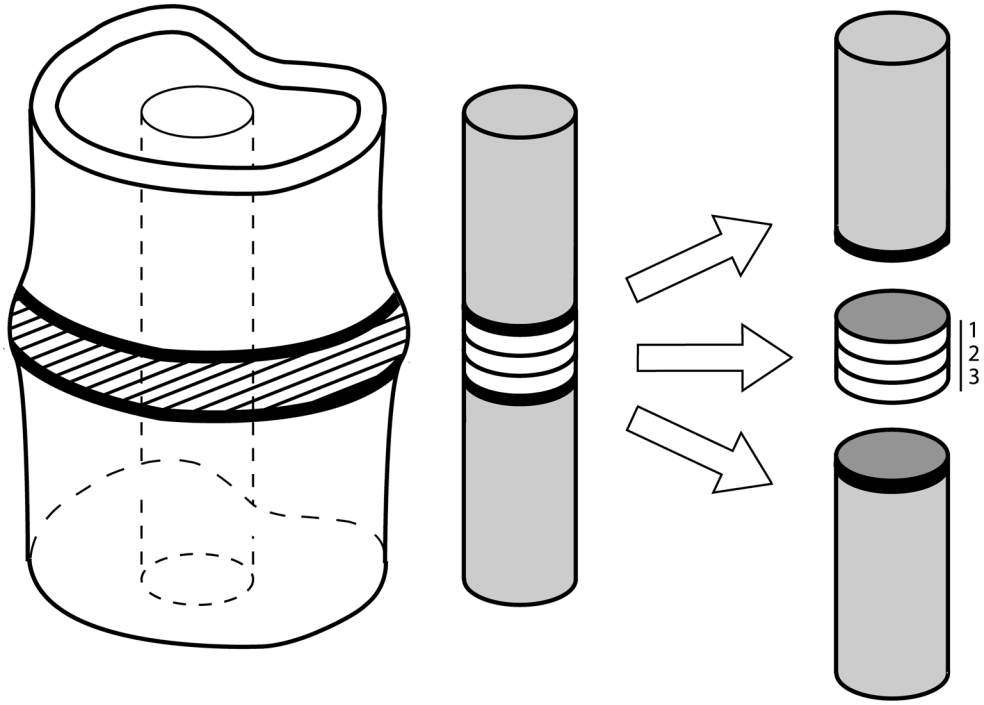

Figure 1.
Schematic of endplate specimen harvest. Specimen is cored from frozen motion segment (8.25 mm diameter). The cartilage endplate attached to the vertebral cores was separated from the nucleus pulposus tissue for microCT (μCT) and permeability measurements. The nuclear tissue was separated in three parts, they are labeled in reference to the adjacent vertebra: inferior (1), center (2), superior (3) for biochemical measurements.

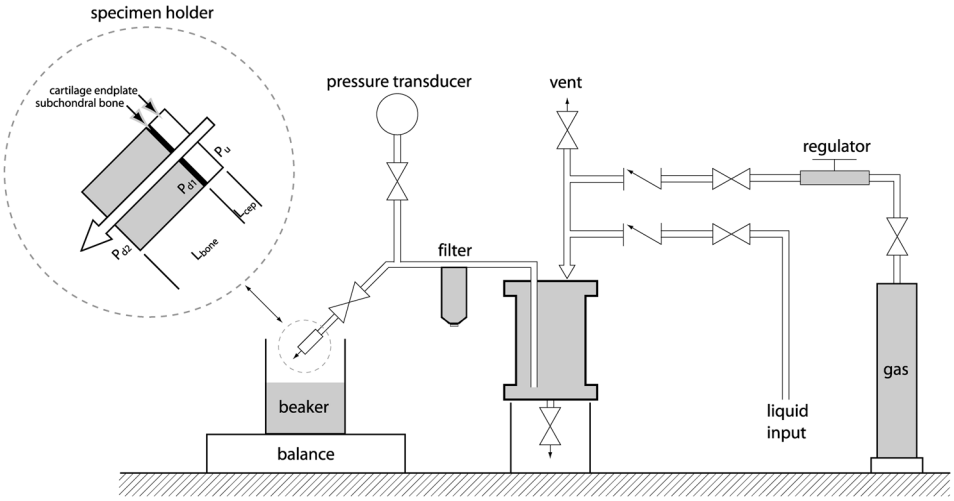

Figure 2.

Illustration of the permeameter. The custom made permeameter is composed of stainless steel pipes connected to a water reservoir. These pipes are also connected to a pressure transducer, a safety pressure release valve, fluid outlets, a filter and a specimen connector. The fluid is pressurized to 1 MPa and pressed through the cartilage-bone specimen. A schematic of the test specimen is shown on the top left corner where P_u is the upstream pressure, P_{d1} is the pressure downstream of the cartilage endplate, and P_{d2} is the pressure downstream of the subchondral bone

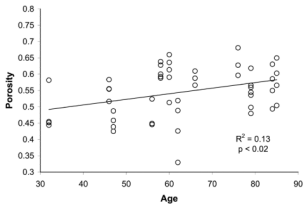

Figure 3.
The variation of subchondral bone porosity with age (R^2=0.13, p=0.004).

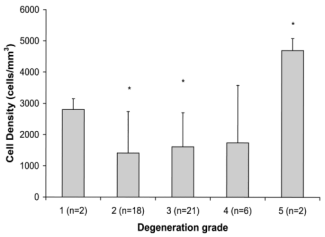

Figure 4.
The variation of cell density (cells/mm^3) with Pfirrmann degeneration grades is presented. Results are shown for mean and standard deviations (Significance using post-hoc Tukey test, *$p<0.05$).

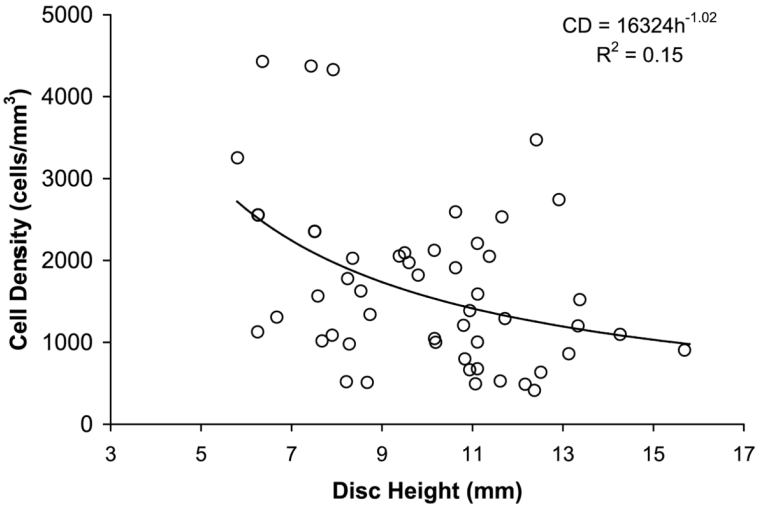

Figure 5.

The variation of cell density (cells/mm^3) with disc height (mm) is shown. Data fitted with a non-linear fit equation of the relationship between the two parameters cell density (CD) and disc height (h); CD =16324 × $h^{-1.02}$ (R^2 = 0.15, p = 0.005).

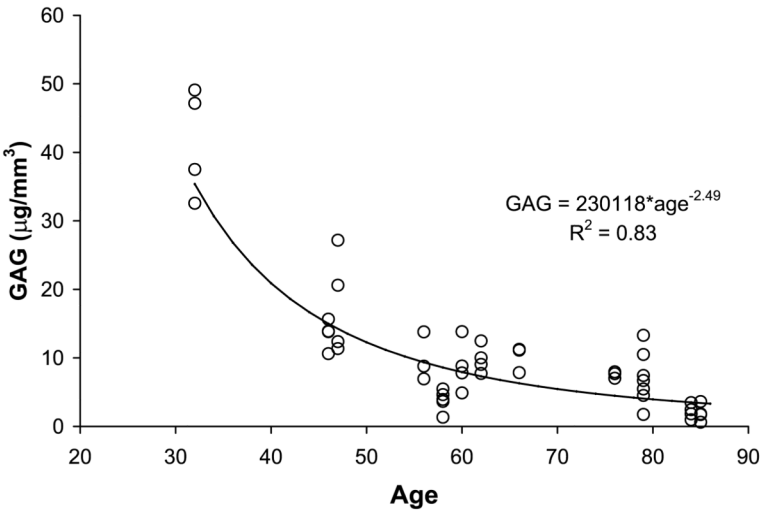

Figure 6.
The variation of GAG content with age is shown. Data fitted with non-linear fit equation of the two variables GAG =230118*age$^{-2.49}$ (R^2 = 0.83, p<0.0001).

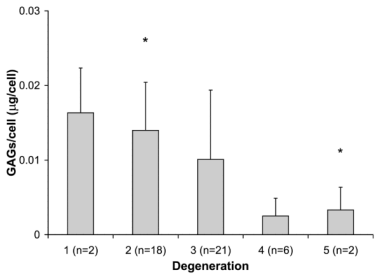

Figure 7.
The variation of cell function (GAGs/cell) was compared to Pfirrmann degeneration grading. Results are shown for mean and standard deviations. (Significance using post-hoc Tukey test, *$p<0.05$)

Table 1

Means and standard deviations for outcome variables

Parameter (units)	Sample size	Mean ± SD
Cell density (cells/mm^3)	50	1650 ± 1015
GAG content (μg/mm^3)	50	10.9 ± 10.6
GAGs/cell (μg/cell)	50	0.0104 ± 0.008
Disc height (mm)	51	10.00 ± 2.31
Total mobility (m^4/N-s)	50	$3.26 \pm 4.43 \times 10^{-10}$
Cartilage mobility (m^4/N-s)	50	$1.19 \pm 1.64 \times 10^{-10}$
Bone mobility (m^4/N-s)	50	$2.21 \pm 13.7 \times 10^{-9}$
Subchondral bone porosity	87	0.54 ± 0.07
Cartilage thickness (mm)	50	1.68 ± 0.59

Table 2

Correlation coefficients between variables (R^2)

	Average GAGs content (μg/mm^3)	Average GAGs/cell (μg/cell)	Pfirrmann Degeneration Scale	Disc Height (mm)	Age	Total mobility (m^4/N-s)	Bone mobility (m^4/N-s)	Cartilage mobility (m^4/N-s)	Porosity	Cartilage thickness (mm)
Average cell density (cells/mm^3)	0.10* p<0.02	0.19** p<0.002	0.24* p<0.014	0.15* p=.005	0.03 p=0.20	0.01 p=0.44	0.06 p=0.1	0.012 p=0.45	0.01 p=0.54	0.01 p=0.52
Average GAGs content (μg/mm^3)		0.22*** p<0.001	0.52*** p<0.0001	0.20*** p<0.001	0.83*** p<0.0001	0.05 p=0.16	0.16** p=0.004	0.05 p=0.15	0.20** p<0.002	0.07 p=0.07
Average GAGs/cell (μg/cell)			0.24*** p<0.0001	0.17** p<0.01	0.14** p<0.01	0.012 p=0.49	0.001 p=0.84	0.05 p=0.31	0.05 p=0.04	0.05 p=0.12
Pfirrmann Degeneration Scale				0.57*** p<0.0001	0.31** p=0.002	0.04 p=0.80	0.066 p=0.53	0.03 p=0.90	0.22** p<0.004	0.01 p=0.38
Disc Height (mm)					0.06 p=0.08	0.001 p=0.90	0.003 p=0.71	0.01 p=0.54	0.01 p=0.65	0.04 p=0.15
Age						0.16** p<0.01	0.10* p=0.03	0.06 p=0.09	0.13** p<0.01	0.08* p=0.03
Total mobility (m^4/N-s)							0.08 p=0.06	0.96** p<0.0001	0.09* p=0.05	0.05 p=0.13
Bone mobility (m^4/N-s)								0.05 p=0.13	0.23*** p<0.001	0.014 p=0.41
Cartilage mobility (m^4/N-s)									0.09* p=0.04	0.01 p=0.58
Porosity										0.05 p=0.13

Significance of correlation

* p<0.05,

** p<0.01,

*** p<0.001